ViSA-Flow: Accelerating Robot Skill Learning via Large-Scale Video Semantic Action Flow

Changhe Chen*1, Quantao Yang*2, Xiaohao Xu1, Nima Fazeli1, Olov Andersson2

¹University of Michigan, ²KTH Royal Institute of Technology

Abstract: One of the central challenges preventing robots from acquiring complex manipulation skills is the prohibitive cost of collecting large-scale robot demonstrations. In contrast, humans are able to learn efficiently by watching others interact with their environment. To bridge this gap, we introduce semantic action flow as a core intermediate representation capturing the essential spatio-temporal manipulator-object interactions, invariant to superficial visual differences. We present ViSA-Flow, a framework that learns this representation self-supervised from unlabeled large-scale video data. First, a generative model is pre-trained on semantic action flows automatically extracted from large-scale human-object interaction video data, learning a robust prior over manipulation structure. Second, this prior is efficiently adapted to a target robot by fine-tuning on a small set of robot demonstrations processed through the same semantic abstraction pipeline. We demonstrate through extensive experiments on the CALVIN benchmark and real-world tasks that ViSA-Flow achieves state-of-the-art performance, particularly in low-data regimes, outperforming prior methods by effectively transferring knowledge from human video observation to robotic execution. Videos are available at https://visaflow-web.github.io/ViSAFLOW.

Keywords: Robot Manipulation, Imitation Learning, Learning from Video

1 Introduction

Robot imitation learning has achieved remarkable success in enabling robots to acquire complex manipulation skills, ranging from basic object manipulation [1, 2] to intricate assembly procedures [3]. However, the scalability of traditional imitation learning approaches is fundamentally limited by the need for extensive, carefully curated robot datasets that are costly to collect. This has become a critical bottleneck in developing robots capable of performing diverse real-world tasks.

In contrast, humans demonstrate an extraordinary ability to learn new skills by observing others. Whether it be in person, instructional videos or even from sports broadcasts, humans instinctively focus on the semantically relevant components. For instance, when learning tennis, we naturally attend to the player's body movements, racquet handling techniques, and ball trajectories, while effectively filtering out irrelevant background information. This selective attention to meaningful elements enables efficient skill acquisition and transfer. The vast repository of publicly available videos on the internet similarly represents an untapped resource for robot learning, offering diverse demonstrations of human skills across countless domains. However, effectively leveraging this resource requires addressing several key challenges, particularly in bridging the gap between human demonstrations in unconstrained videos and robot execution in the real world.

Recent research [4, 5, 6] has explored enabling robots to acquire skills by directly observing unstructured human videos. These approaches have demonstrated strong generalizability, allowing robots to adapt to new tasks effectively. In most real-world scenarios, when humans learn a skill, we primarily focus on the interaction between the human hand (or arm) and the manipulated object, while disregarding irrelevant background elements or distractions. Mimicking this selective attention mechanism could enhance the efficiency and effectiveness of robot learning from videos.

^{*}Equal contribution. Corresponce to: changhec@umich.edu, quantao@kth.se.

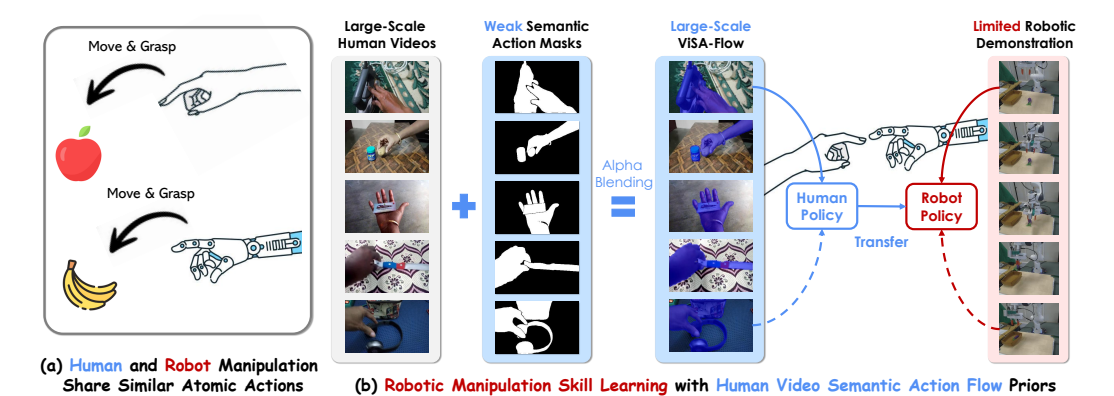


Figure 1: Learning Robot Manipulation Skills from Human Videos via Semantic Action Transfer. (a) Humans and robots often share underlying atomic actions for similar tasks (e.g., Move & Grasp). (b) Our framework leverages large-scale, unlabeled human videos by extracting weakly supervised semantic action flow priors (ViSA-Flow). This knowledge is distilled into a human policy and efficiently transferred to learn a corresponding robot policy.

Drawing inspiration from this, we propose a novel approach that enables robots to learn skills by extracting and leveraging semantic representations from large-scale video collections. Our framework outlined in Fig. 1 focuses on identifying the key semantic elements relevant to skill acquisition, much like how humans naturally attend to meaningful components while learning from visual demonstrations. By concentrating on these semantic features - such as object interactions, body poses, and motion patterns - rather than processing entire scenes indiscriminately, our approach aims to make video-based skill learning more efficient and generalizable. Our key contributions are threefold:

- 1. We propose ViSA-Flow, a framework for pre-training generative policies using large-scale Video Semantic Action Flow, capturing spatio-temporal manipulator-object interactions from diverse human video demonstrations. This enables efficient knowledge transfer from Internet-scale human video data to robotic manipulation policies.
- We refine the pretrained policy using robot-specific semantic actions from few expert demonstrations by tracking hand-object interactions in both human videos and robot data, enabling robust semantic alignment for improved policy adaptation.
- 3. We evaluate ViSA-Flow in both simulated and real-world robotic manipulation tasks, demonstrating substantial performance improvements over SOTA baselines. Our method boosts task success rates, highlighting the effectiveness of video-driven robot skill learning.

2 Related Work

Visual-Feature-Based Imitation Learning. Recent advancements [7, 8, 9, 10, 11] in visual feature-based imitation learning have significantly improved the efficiency, generalization, and robustness of learning from visual demonstrations. VIEW [12] introduces a trajectory segmentation approach that extracts condensed prior trajectories from demonstrations, allowing robots to learn manipulation tasks more efficiently. Similarly, K-VIL [13] enhances efficiency by extracting sparse, object-centric keypoints from visual demonstrations, reducing redundancy and improving learning speed. Beyond efficiency, generalization remains a critical challenge, particularly in adapting to diverse visual environments. Stem-OB [14] addresses this issue by leveraging diffusion model inversion to suppress low-level visual differences, improving robustness against variations in lighting and texture. In addition, goal-oriented approaches have been developed to improve policy learning and adaptation. Visual hindsight self-imitation learning [15] introduces hindsight goal re-labeling and prototypical goal embedding, enhancing sample efficiency in vision-based tasks.

Video-Based Robot Learning. Recent advancements [16, 17, 18, 19] in robot learning have demonstrated the effectiveness of large-scale video datasets for pre-training models and improving gener-

alization. Methods such as Time-Contrastive Networks (TCN) [20] have pioneered the extraction of temporally consistent features to align human demonstrations with robot actions. Building on this foundation, video pretraining [21] has shown that large-scale video data can be used to pretrain robust visual representations for downstream manipulation tasks. More recent works [22] have further leveraged large-scale video datasets to enhance manipulation performance. Similarly, Vid2Robot [23] presents an end-to-end framework that directly translates video demonstrations and real-time observations into robot actions, leveraging cross-attention mechanisms for improved alignment. [6] highlights the potential of leveraging partially-annotated data to enhance robot policy learning by integrating multi-modal information.

3 Method

Our approach facilitates learning robot manipulation policies from limited *target-domain* data by leveraging knowledge distilled from large-scale *source-domain* (human) videos. This is achieved through the introduction and utilization of **Video Semantic Action Flow (ViSA-Flow)**, a structured intermediate representation designed for cross-domain transfer. We first formulate the conceptual properties of ViSA-Flow and motivate its suitability for transfer learning, then detail its concrete implementation within our two-stage learning framework.

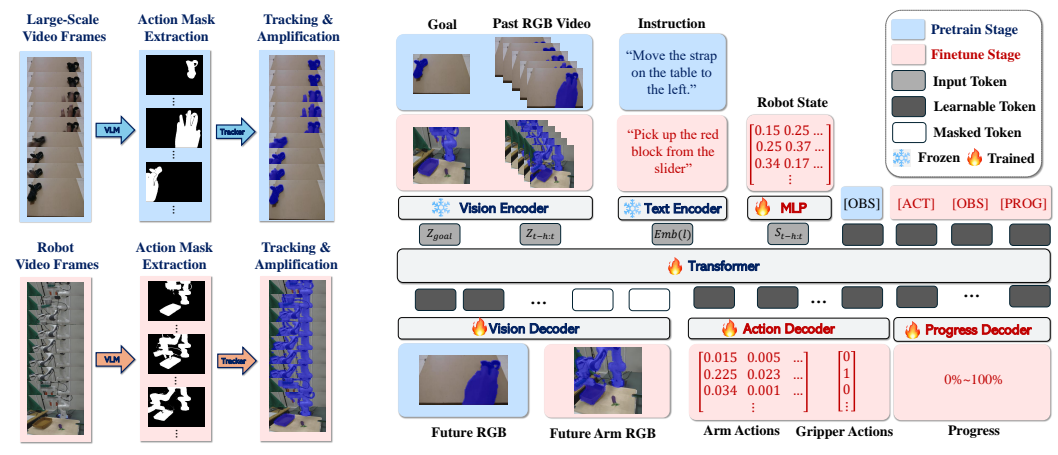
3.1 Problem Definition

Our objective is to pretrain a policy model π_{θ} by utilizing human-object interactions from a large dataset of human manipulation videos, $D_v = \{v_i\}^M$. This pretraining aims to facilitate learning on a target robotic task using only a small dataset of robot demonstrations, $D_{\tau} = \{\tau_j\}^N$, where $N \ll M$. The target task involves controlling a robot based on language instructions, observations, and proprioceptive state. We define the robot's observation space as O, its proprioceptive state space as S, and its action space as A. Given a language instruction l, our goal is to learn a policy $\pi_{\theta}(a_t|l,o_{t-h:t},s_{t-h:t})$ that outputs an action $a_t \in A$ based on the instruction l, a history of recent observations $o_{t-h:t} \in O$, and recent states $s_{t-h:t} \in S$. This policy is learned primarily by imitating the demonstrations in D_{τ} , leveraging the pretraining from D_v .

3.2 ViSA-Flow Representation

We propose ViSA-Flow as an intermediate representation $z_t \in Z_{\text{ViSA-Flow}}$ obtained by mapping an observation o_t and context l through a function $f: O \times L \to Z_{\text{ViSA-Flow}}$. The motivation is to define a representation space $Z_{\text{ViSA-Flow}}$ where the manipulation interaction relevant to the task is preserved while the domain-specific nuisance factors are mitigated, facilitating skill transfer from O^S to O^T .

- 1) Semantic Entity Grounding. Given the initial observation frame o_0 and context l, we utilize a pre-trained Vision-Language Model (VLM) to ground textual descriptions of the manipulator (e.g., 'hand', 'gripper') and task-relevant objects (e.g., 'red block') identified from l. A segmentation model (e.g., SAM [24]) then generates initial segmentation masks for these grounded entities, including manipulators and objects, *i.e.*, $\{m_{M,0}, m_{O_k,0}\}$.
- 2) Hand-Object Interaction Tracking. Due to the instability of semantic segmentation across sequential frames, we propose tracking the correctly segmented hand-object interaction mask over time. Specifically, we instantiate a robust point tracker (e.g., CoTracker [25]) with points densely sampled within the initial masks. The tracker estimates the 2D image trajectories $P_t = \{p_{j,t}\}_{j=0}^N$ for these points across the sequence $\{o_t\}_{t=0}^T$. These trajectories P_t represent the extracted raw flow information, capturing the motion of key interaction points.
- 3) Flow-Conditioned Feature Encoding. To produce the final VISA-Flow representation z_t , we encode the flow information P_t into a rich feature vector while retaining visual context. We first apply a perceptual enhancement process directly on the raw observation frame o_t . Using tracked point



(a) Video Semantic Action Flow Construction

(b) Policy Learning with Large-Scale Video Semantic Action Flow

Figure 2: ViSA-Flow Architecture and Policy Learning Framework. (a) During pretraining, hand-object interaction masks are extracted from large-scale video frames and amplified via tracking to generate semantic flow representations. (b) In the finetuning stage, a multi-modal Transformer architecture conditions on the goal image, a sequence of RGB observation frames enhanced with pre-trained ViSA-Flow, language instructions and robot state. The Transformer predicts future visual states, low-level robot actions, and task progress using dedicated decoders.

trajectories P_t , we generate a spatially-localized amplification mask $M_t(x, y)$ with parameterized radius r around each tracker coordinate:

$$M_t(x,y) = \max_{p \in P_t} \mathbf{1}(\|(x,y) - p\|_2 \le r).$$
 (1)

This mask modulates pixel intensities by an amplification factor α within these regions of interest, while maintaining contextual information elsewhere. The resulting perceptually-enhanced frame exhibits selective luminance amplification at interaction-critical regions. This pre-processed frame is then passed through a vision encoder ϕ (e.g., MAE [26]), transforming the flow-highlighted observations into our implemented ViSA-Flow representation z_t :

$$z_t = \phi(o_t \odot [1 + \alpha M_t]). \tag{2}$$

This implementation aims to focus on tracked semantic entities and modulating features accordingly.

3.3 Policy Learning through ViSA-Flow Representation

Our learning framework leverages the extracted ViSA-Flow representations z_t within a two-stage pre-training and fine-tuning scheme, implemented using a transformer architecture, denoted g_{ψ} (parameters ψ), inspired by prior work such as GR-1 [22].

Model Architecture. A transformer g_{ψ} is designed to process multimodal sequences for both generative prediction and policy inference shown in Fig. 2. Its input is a sequence formed by concatenating tokens representing various modalities and special learnable query tokens. Primary input modalities include language instruction embeddings $\operatorname{Emb}(l)$ (e.g., from CLIP [27]), the sequence of recent ViSA-Flow representations $\{z_{t-h},...,z_t\}$ encoding flow-conditioned visual features (Sec. 3.2), the sequence of proprioceptive states $\{s_{t-h},...,s_t\}$ (processed via linear embeddings), and potentially tokens representing a goal state z_{goal} . Added to these are special query tokens: an [ACT] token for action prediction and multiple [0BS] tokens for predicting future ViSA-Flow states. Standard positional embeddings are added to this combined sequence to encode temporal order before processing by the transformer blocks. The output embeddings corresponding to the query tokens are then directed to task-specific heads; notably, the [ACT] token's output yields the action chunk prediction $\hat{a}_{t+1:t+k}$, while the [0BS] tokens' outputs yield predictions $\hat{z}_{t+1:t+n}$ for future states.

Stage 1: Pre-training – Learning ViSA-Flow Dynamics Prior. Using the large-scale human video dataset D_v , we pre-train g_ψ to model the dynamics within the ViSA-Flow space. For each sequence $v_i \in D_v$, we extract $\{z_{i,t}\}$ (Sec. 3.2). The model is trained to predict future representations $z_{t+1:t+n}$ based on past context $z_{\leq t}$ and l, using the [OBS] query tokens. The objective is to minimize the prediction error, typically via Mean Squared Error (MSE):

$$\mathcal{L}_{\text{pretrain}}(\psi) = \mathbb{E}_{v \sim D_v} \left[||g_{\psi}(z_{< t}, l)_{\text{[OBS]}} - z_{t+1:t+n}||^2 \right]. \tag{3}$$

This stage yields pre-trained parameters $\psi_{\rm pre}$, encoding a prior over interaction dynamics.

Stage 2: Fine-tuning – Policy Adaptation. Using the small-scale robot demonstration dataset D_{τ} , we fine-tune the model, initialized with ψ_{pre} , to learn the target policy π_{θ} (where $\theta \subseteq \psi$). For each robot trajectory $\tau_{j} \in D_{\tau}$, we extract ViSA-Flow representations $\{z_{j,t}\}$ using the identical pipeline. The model is trained end-to-end with a multi-task objective combining action prediction and continued dynamics modeling:

$$\mathcal{L}_{\text{finetune}}(\psi) = \mathbb{E}_{\tau \sim D_{\tau}} \left[\mathcal{L}_{\text{act}}(a_{t+1:t+k}, \hat{a}_{t+1:t+k}) + \lambda_{\text{fwd}} \mathcal{L}_{\text{obs}}(z_{t+1:t+n}, \hat{z}_{t+1:t+n}) + \lambda_{\text{prog}} \mathcal{L}_{\text{prog}}(p_t, \hat{p}_t) \right]. \tag{4}$$

Here, $\hat{a}_t = g_{\psi}(z_{\leq t}, s_{\leq t}, l)_{[ACT]}$ is the predicted action. \mathcal{L}_{act} is the action loss (e.g., a weighted combination of Smooth L1, BCE, KL divergence terms appropriate for the action space). $\hat{z}_{t+1:t+n} = g_{\psi}(z_{\leq t}, s_{\leq t}, l)_{[OBS]}$ are predicted future ViSA-Flow states, and \mathcal{L}_{obs} is the forward dynamics loss (MSE, identical form to Eq. 3 but on D_{τ}) weighted by λ_{fwd} . \hat{p}_t is the optional predicted progress, with \mathcal{L}_{prog} being the progress loss (e.g., MSE) weighted by λ_{prog} . This stage adapts the general dynamics prior to the specific robot and learns the mapping from ViSA-Flow states (and proprioception) to robot actions, yielding the final policy parameters ψ .

4 Evaluation

We conduct extensive experiments in both simulated and real-world environments to systematically evaluate ViSA-Flow's performance. Our evaluation is designed to answer the following key questions: 1) Can ViSA-Flow effectively learn and generalize across multiple tasks, particularly in challenging scenarios involving distractors, different backgrounds, and new objects? 2) Can ViSA-Flow effectively learn and generalize across diverse tasks using minimal expert demonstration data, particularly in scenarios where expert demonstration data with language annotations are scarce? 3) Do semantic actions extracted from human demonstrations benefit robot skill learning?

4.1 Simulation Experiments

Evaluation Setup. We evaluate ViSA-Flow on the CALVIN benchmark [28], a standard testbed for long-horizon, language-conditioned manipulation requiring generalization. We use the ABC \rightarrow D split, training on environments A, B, C and evaluating zero-shot on the unseen environment D as shown in the lower row of Fig. 3.

Pre-training Data. The ViSA-Flow model undergoes pre-training (Stage 1, Sec. 3.3) using the large-scale Something-Something-V2 (SthV2) dataset [29] as the source domain. SthV2 contains approximately 220,000 short videos depicting diverse human-object interactions (examples visualized in the upper row of Fig. 3). Each video is associated with a template-based textual description indicating the action performed (e.g., 'Pushing [something] from left to right') and includes place-holder labels identifying key objects within frames. The videos are processed to extract ViSA-Flow representations which are used for the pre-training as described in Secs. 3.2 and 3.3.

Fine-tuning Data. Following pre-training, ViSA-Flow is fine-tuned (Stage 2, Sec. 3.3) specifically for the CALVIN environment. To evaluate performance under data scarcity, we utilize only **10%** (1,768 trajectories) of the available language-annotated robot demonstrations from CALVIN's ABC dataset as our target domain dataset. Each trajectory consists of the language instruction and the sequence of robot states, observations, and actions.

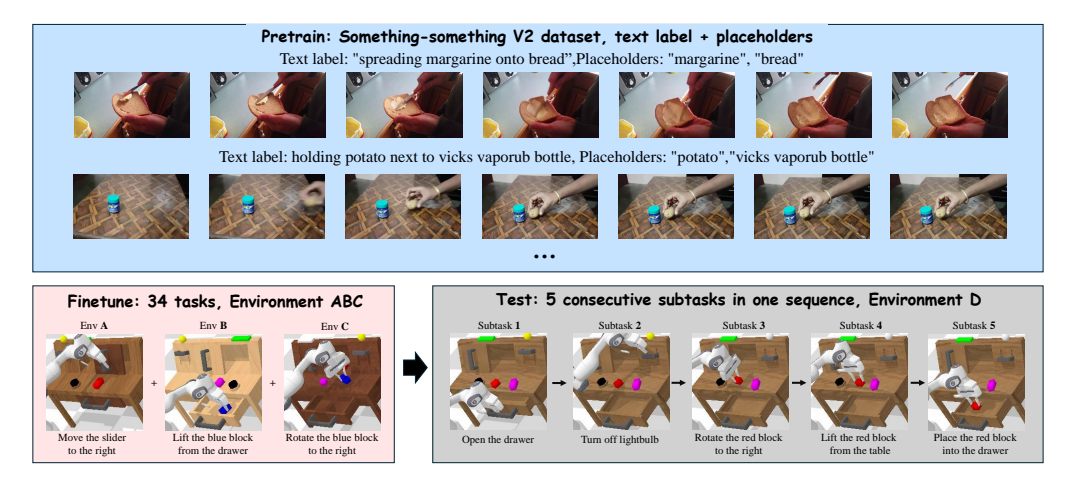


Figure 3: **Datasets used for pretraining, finetuning, and evaluation.** A model is trained on the Something-Something-V2 dataset with text labels. Placeholders are used to extract underlying semantic action flow. The finetuning stage involves 34 manipulation tasks across three simulated environments (Env A, B, and C) in CALVIN benchmark [28]. The evaluation is on Environment D, where the robot complete 5 consecutive subtasks within one continuous sequence.

Table 1: Comparative evaluation on CALVIN ABC \rightarrow D benchmark. Performance metrics include success rates for completing 1-5 consecutive tasks and average sequence length (Avg. Len). Methods in the top section use 100% of training data, while methods in the bottom section use only 10%. The robot executed 1,000 test sequences with five tasks each. **Bold** indicates best performance.

Method	Fully-Annotated	Partially-Annotated Data	Tasks Completed in A Row					Avg. Len.
	Data (Demo No.)		1	2	3	4	5	
Hulc [10]	100% (17870)	✓	41.8%	16.5%	5.7%	1.9%	1.1%	0.67
MDT [17]	100% (17870)	✓	61.7%	40.6%	23.8%	14.7%	8.7%	1.54
Spil [18]	100% (17870)	✓	74.2%	46.3%	27.6%	14.7%	8.0%	1.71
Roboflamingo [19]	100% (17870)	×	82.4%	61.9%	46.6%	33.1%	23.5%	2.47
SuSIE [11]	100% (17870)	✓	87.0%	69.0%	49.0%	38.0%	26.0%	2.69
CLOVER [8]	10% (1768)	X	44.3%	18.0%	5.0%	1.0%	0.0%	0.68
GR-1 [22]	10% (1768)	×	67.2%	37.1%	19.8%	10.8%	6.9%	1.41
SeeR [7]	10% (1768)	×	65.5%	38.8%	21.4%	11.7%	6.8%	1.44
GR-MG [6]	10% (1768)	X	81.8%	59.0%	39.0%	24.0%	16.2%	2.20
ViSA-Flow (Ours)	10% (1768)	X	89.0%	73.8%	56.8%	44.8%	31.4%	2.96

Baselines. We compare ViSA-Flow against two groups of SOTA methods: (i) Low-Data Baselines: Strong contemporary methods trained under the identical 10% data condition as ViSA-Flow for direct comparison of data efficiency. This includes CLOVER [8], GR-1 [22], SeeR[7] and GR-MG [6]. (ii) Full-Data Baselines: Methods trained on 100% of CALVIN annotated robot data (17,870 trajectories), including Hulc [10], MDT [17], Spil [18], Roboflamingo [19] and SuSIE [11]. These represent the performance achievable with substantially more in-domain supervision.

Metrics. Following the standard CALVIN evaluation protocol, we measure the success rate to complete 5 consecutive subtasks within a longer instruction sequence, evaluated over 1,000 independent sequences. We also report the average successful sequence length (Avg. Len.). These metrics assess single-task proficiency and the ability to maintain performance over long horizons.

Results and Analysis. Table 1 presents the performance metrics for all methods. The results demonstrate that ViSA-Flow outperforms all baseline methods, achieving highest success rates across all consecutive task completion metrics despite using only 10% of the available annotated robot trajectories. Most impressively, ViSA-Flow maintains strong performance in sequential tasks, completing 5 consecutive tasks 31.4% of the time, almost twice the rate of the next best method trained with 10% data (GR-MG: 16.2%) and exceeding all methods trained on 100% data, including Susie (26.0%). The average sequence length of 2.96 further demonstrates the effectiveness of ViSA-Flow in handling long-horizon manipulation tasks. Performance degradation from single to sequential tasks

Table 2: Ablation study evaluating the contribution of key components in ViSA-Flow.

Method		Avg. Len.				
1/1001100	1	2	3	4	5	
ViSA-Flow w/o Seg.	71.3%	45.1%	24.5%	14.5%	9.6%	1.64
ViSA-Flow w/o Trace.	87.2%	69.2%	52.0%	39.6%	30.0%	2.78
ViSA-Flow w/o Hand	89.0%	71.8%	54.2%	39.4%	28.4%	2.83
ViSA-Flow (Full)	89.0%	73.8%	56.8%	44.8%	31.4%	2.96

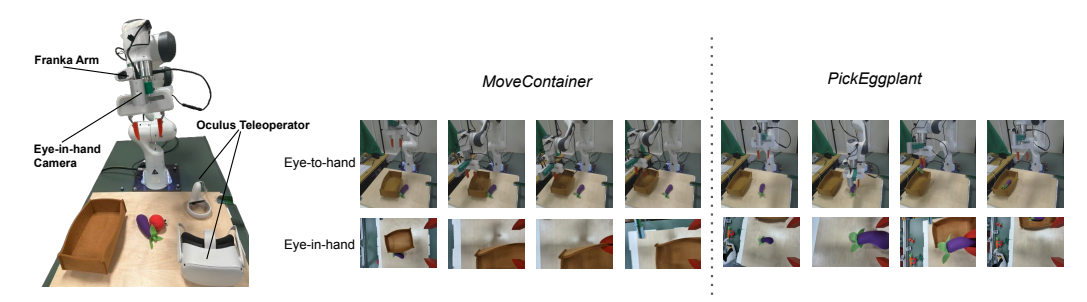


Figure 4: **The real-world experiment setup.** We evaluate ViSA-Flow on two single-stage manipulation tasks and a two-stage long-horizon manipulation task.

 $(89.0\% \rightarrow 31.4\%)$ is notably less severe for ViSA (64.7% reduction) compared to GR-MG (80.2% reduction) and Susie (70.1% reduction). This remarkable performance can probably be attributed to utilization of semantic action representations extracted from human demonstration videos. These results in simulation experiments validate our hypothesis that semantic action representations from human videos can significantly enhance robot skill learning, even when expert demonstrations are scarce and encounter different environments.

Ablation Study of ViSA-Flow Components. Table 2 summarizes the results when each component within the ViSA-Flow framework is individually removed from the full method. Removing the semantic entity grounding stage and tracking the motion of points across whole observation images significantly reduces performance across all consecutive-task metrics. Success rate on five-task sequences drops from 31.4% to just 9.6% with the average successful length falling from 2.96 to 1.64, which indicates the importance of accurately segmenting and identifying semantic entities to anchor tracking and flow conditioning. Omitting the robust temporal tracking stage decreases the average successful length over five-task sequences from 2.96 to 2.78, highlighting that consistent point correspondences are essential for preserving temporal dynamics across multi-step interactions. Excluding explicit manipulator grounding results in a modest drop in average sequence length, from 2.96 to 2.83, indicating that while segmentation and tracking are primary drivers of performance, manipulator cues still play a meaningful role in providing spatial context for action understanding. Overall, the full ViSA-Flow configuration—integrating segmentation, tracking, and manipulator grounding—achieves the best results across all metrics, confirming that each component contributes to capturing semantic action flow and enabling reliable long-horizon, cross-domain task execution.

4.2 Real World Experiments

We evaluate the performance of ViSA-Flow in real-world experiments across diverse settings, focusing on its effectiveness and robustness in solving both single-stage and long-horizon tasks.

Experiment Setup. We evaluate our ViSA-Flow method in two real-world settings: two single-stage manipulation tasks and one long-horizon manipulation task. The demonstrations were collected by teleoperating a 7-DOF Franka Emika Panda arm using the Oculus-based application. We use two cameras (one eye-in-hand, one eye-to-hand) to provide RGB observations. The real-world experiment setup is shown in Fig. 4. For single-stage tasks, we collected 46 and 54 demonstrations for two tasks—*MoveContainer* and *PickEggplant* respectively. We train the ViSA-Flow policy for each single-stage task. For long-horizon tasks, we consider the same two subtasks, *MoveContainer*

and *PickEggplant*, requiring the robot to complete the first task before sequentially solving the second. This setup ensures consistency with the testing scenario used in our simulation experiments. We evaluate each policy across 12 different initial positions.

Baselines. We compare our ViSA-Flow method with GR-MG [6] and the visuomotor Diffusion Policy (DP) [30], which leverages both RGB and proprioceptive inputs. To ensure fair comparison, all baseline models are trained on the same real-world demonstration datasets for the two single-stage tasks and the long-horizon task.

Quantitative Results and Analysis. The real-world experimental results are presented in Fig. 5. For the single-stage tasks *MoveContainer* and *PickEggplant*, ViSA-Flow significantly outperforms the GR-MG model across 12 trials. Meanwhile, DP achieves a comparable success rate of 75.0% on the *PickEggplant* task. In contrast, for the long-horizon task—which sequentially combines *MoveContainer* and *PickEggplant*—our method demon-



Figure 5: **Real-world experimental results**. **Left**: two single-stage tasks; **Right**: a two-stage long-horizon task.

strates superior performance, achieving 9/12 successful trials for each subtask and yielding an overall success rate of 56.3% for the full sequence. By comparison, GR-MG and DP attain success rates of only 8.3% and 13.8%, respectively. Notably, DP experiences a significant performance drop when transitioning from single-stage to long-horizon tasks, whereas ViSA-Flow maintains robust and consistent performance.

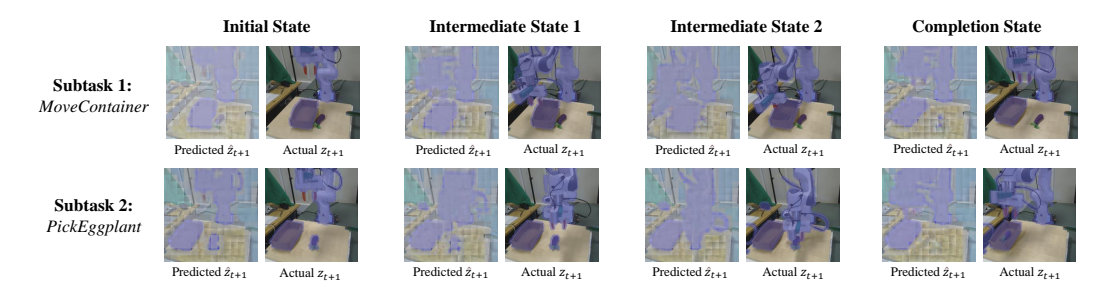


Figure 6: Qualitative results on the real world long-horizon task. We visualize the decoded ViSA-Flow prediction at \hat{z}_{t+1} against the actual ViSA-Flow z_{t+1} extracted from the next observation for four execution phases. Two rows correspond to the two subtasks that make up the long-horizon evaluation: (Top) Subtask 1 – MoveContainer. (Bottom) Subtask 2 – PickEggplant. Qualitatively, the model's one-step predictions closely follow the true motion of the manipulator and task-relevant objects, even as the scene evolves across distinct interaction stages.

Qualitative Results and Analysis. Fig. 6 qualitatively demonstrates that the decoded ViSA-Flow one-step prediction \hat{z}_{t+1} remains tightly aligned with the ground-truth flow throughout the entire long-horizon execution: the model persistently focuses on the robot gripper and the task-relevant objects while suppressing background clutter, its spatial support evolves smoothly and coherently as the scene transitions from the initial approach, through two intermediate contact phases, to the completion state, and the same level of accuracy is observed across the two sequential subtasks. This close match between prediction and observation confirms that the cross-domain dynamics prior learned during pretraining effectively captures task-critical interaction structure and generalizes to novel real-world embodiments.

5 Limitations and Future Work

While ViSA-Flow demonstrates strong performance in observational robot learning, it currently lacks explicit modeling of 3D geometry and contact dynamics, which may limit its generalization to tasks involving fine-grained physical interactions. The current framework also relies on pretrained VLM components that potentially restrict adaptability to novel domains. Future work includes enriching ViSA-Flow representations with contact physics and reducing reliance on pretrained components by jointly training ViSA-Flow with VLMs. Additionally, integrating ViSA-Flow's priors with reinforcement learning algorithms and scaling pretraining to web-scale video corpora offer promising directions for advancing generalizable robot learning.

References

- [1] A. Hussein, M. M. Gaber, E. Elyan, and C. Jayne. Imitation learning: A survey of learning methods. *ACM Computing Surveys (CSUR)*, 50(2):1–35, 2017.
- [2] T. Gao, S. Nasiriany, H. Liu, Q. Yang, and Y. Zhu. Prime: Scaffolding manipulation tasks with behavior primitives for data-efficient imitation learning. *arXiv preprint arXiv:2403.00929*, 2024.
- [3] C. Chi, Z. Xu, S. Feng, E. Cousineau, Y. Du, B. Burchfiel, R. Tedrake, and S. Song. Diffusion policy: Visuomotor policy learning via action diffusion. *The International Journal of Robotics Research*, page 02783649241273668, 2023.
- [4] S. Bahl, A. Gupta, and D. Pathak. Human-to-robot imitation in the wild. *arXiv preprint* arXiv:2207.09450, 2022.
- [5] J. Zeng, Q. Bu, B. Wang, W. Xia, L. Chen, H. Dong, H. Song, D. Wang, D. Hu, P. Luo, et al. Learning manipulation by predicting interaction. *arXiv preprint arXiv:2406.00439*, 2024.
- [6] P. Li, H. Wu, Y. Huang, C. Cheang, L. Wang, and T. Kong. Gr-mg: Leveraging partially-annotated data via multi-modal goal-conditioned policy. *IEEE Robotics and Automation Letters*, 2024.
- [7] Y. Tian, S. Yang, J. Zeng, P. Wang, D. Lin, H. Dong, and J. Pang. Predictive inverse dynamics models are scalable learners for robotic manipulation, 2024. URL https://arxiv.org/ abs/2412.15109.
- [8] Q. Bu, J. Zeng, L. Chen, Y. Yang, G. Zhou, J. Yan, P. Luo, H. Cui, Y. Ma, and H. Li. Closed-loop visuomotor control with generative expectation for robotic manipulation, 2024. URL https://arxiv.org/abs/2409.09016.
- [9] Q. Yang, M. C. Welle, D. Kragic, and O. Andersson. S²-diffusion: Generalizing from instance-level to category-level skills in robot manipulation. *arXiv preprint arXiv:2502.09389*, 2025.
- [10] O. Mees, L. Hermann, and W. Burgard. What matters in language conditioned robotic imitation learning over unstructured data, 2022. URL https://arxiv.org/abs/2204.06252.
- [11] K. Black et al. Zero-shot robotic manipulation with pretrained image-editing diffusion models. *arXiv preprint arXiv:2310.10639*, 2023.
- [12] A. Jonnavittula, S. Parekh, and D. P. Losey. View: Visual imitation learning with waypoints, 2025. URL https://arxiv.org/abs/2404.17906.
- [13] J. Gao, Z. Tao, N. Jaquier, and T. Asfour. K-vil: Keypoints-based visual imitation learning. IEEE Transactions on Robotics, 39(5):3888–3908, Oct. 2023. ISSN 1941-0468. doi:10.1109/tro.2023.3286074. URL http://dx.doi.org/10.1109/TRO.2023.3286074.

- [14] K. Hu, Z. Rui, Y. He, Y. Liu, P. Hua, and H. Xu. Stem-ob: Generalizable visual imitation learning with stem-like convergent observation through diffusion inversion, 2024. URL https://arxiv.org/abs/2411.04919.
- [15] K. Kim, M. Lee, M. Whoo Lee, K. Shin, M. Lee, and B.-T. Zhang. Visual hindsight self-imitation learning for interactive navigation. *IEEE Access*, 12:83796–83809, 2024. ISSN 2169-3536. doi:10.1109/access.2024.3413864. URL http://dx.doi.org/10.1109/ACCESS.2024.3413864.
- [16] A. Brohan et al. Rt-2: Vision-language-action models transfer web knowledge to robotic control. *arXiv preprint arXiv:2307.15818*, 2023.
- [17] M. Reuss, Ömer Erdinç Yağmurlu, F. Wenzel, and R. Lioutikov. Multimodal diffusion transformer: Learning versatile behavior from multimodal goals, 2024. URL https://arxiv.org/abs/2407.05996.
- [18] H. Zhou, Z. Bing, X. Yao, X. Su, C. Yang, K. Huang, and A. Knoll. Language-conditioned imitation learning with base skill priors under unstructured data, 2024. URL https://arxiv.org/abs/2305.19075.
- [19] X. Li, M. Liu, H. Zhang, C. Yu, J. Xu, H. Wu, C. Cheang, Y. Jing, W. Zhang, H. Liu, H. Li, and T. Kong. Vision-language foundation models as effective robot imitators, 2024. URL https://arxiv.org/abs/2311.01378.
- [20] P. Sermanet, C. Lynch, Y. Chebotar, J. Hsu, E. Jang, S. Schaal, and S. Levine. Time-contrastive networks: Self-supervised learning from video, 2018. URL https://arxiv.org/abs/1704.06888.
- [21] B. Baker, I. Akkaya, P. Zhokhov, J. Huizinga, J. Tang, A. Ecoffet, B. Houghton, R. Sampedro, and J. Clune. Video pretraining (vpt): Learning to act by watching unlabeled online videos, 2022. URL https://arxiv.org/abs/2206.11795.
- [22] H. Wu, Y. Jing, C. Cheang, G. Chen, J. Xu, X. Li, M. Liu, H. Li, and T. Kong. Unleashing large-scale video generative pre-training for visual robot manipulation, 2023. URL https://arxiv.org/abs/2312.13139.
- [23] V. Jain, M. Attarian, N. J. Joshi, A. Wahid, D. Driess, Q. Vuong, P. R. Sanketi, P. Sermanet, S. Welker, C. Chan, I. Gilitschenski, Y. Bisk, and D. Dwibedi. Vid2robot: End-to-end videoconditioned policy learning with cross-attention transformers, 2024. URL https://arxiv. org/abs/2403.12943.
- [24] A. Kirillov et al. Segment anything. arXiv preprint arXiv:2304.02643, 2023.
- [25] N. Karaev, I. Makarov, J. Wang, N. Neverova, A. Vedaldi, and C. Rupprecht. Cotracker3: Simpler and better point tracking by pseudo-labelling real videos, 2024. URL https://arxiv.org/abs/2410.11831.
- [26] K. He, X. Chen, S. Xie, Y. Li, P. Dollár, and R. Girshick. Masked autoencoders are scalable vision learners, 2021. URL https://arxiv.org/abs/2111.06377.
- [27] A. Radford, J. W. Kim, C. Hallacy, A. Ramesh, G. Goh, S. Agarwal, G. Sastry, A. Askell, P. Mishkin, J. Clark, G. Krueger, and I. Sutskever. Learning transferable visual models from natural language supervision, 2021. URL https://arxiv.org/abs/2103.00020.
- [28] O. Mees, L. Hermann, E. Rosete-Beas, and W. Burgard. Calvin: A benchmark for language-conditioned policy learning for long-horizon robot manipulation tasks. *IEEE Robotics and Automation Letters (RA-L)*, 7(3):7327–7334, 2022.

- [29] R. Goyal, S. E. Kahou, V. Michalski, J. Materzyńska, S. Westphal, H. Kim, V. Haenel, I. Fruend, P. Yianilos, M. Mueller-Freitag, F. Hoppe, C. Thurau, I. Bax, and R. Memisevic. The "something something" video database for learning and evaluating visual common sense, 2017. URL https://arxiv.org/abs/1706.04261.
- [30] C. Chi, S. Feng, Y. Du, Z. Xu, E. Cousineau, B. Burchfiel, and S. Song. Diffusion policy: Visuomotor policy learning via action diffusion. In *Proceedings of Robotics: Science and Systems (RSS)*, 2023.

A Appendix

A.1 More Details about ViSA-Flow Representation

Desired Properties of ViSA-Flow. We hypothesize that an effective ViSA-Flow representation $z_t = f(o_t, l)$ should possess the following properties:

- 1. **Encodes Interaction Structure:** z_t should explicitly encode the essential spatio-temporal relationships and relative motions between the primary manipulator (hand/gripper) and the key objects involved in the manipulation task described by l.
- 2. Invariance to Visual Nuisance Factors: The mapping f should be robust to variations in o_t that are irrelevant to the core interaction semantics, such as background clutter, lighting conditions, or specific object/manipulator textures. Formally, for a nuisance variation δ_O , we desire $f(o_t, l) \approx f(o_t + \delta_O, l)$.
- 3. Cross-Domain Alignment of Task Structure: Despite morphological and appearance differences between source (O^S) and target (O^T) domains, many manipulation tasks share fundamental geometric and dynamic structures. ViSA-Flow should align these structures. If o_t^S and o_t^T depict the same semantic phase of a task (e.g., pre-grasp approach), their representations $z_t^S = f(o_t^S, l)$ and $z_t^T = f(o_t^T, l)$ should be proximate in $Z_{\text{ViSA-Flow}}$ under a suitable metric d, i.e., $d(z_t^S, z_t^T) \approx 0$.

Motivation for Transfer Learning via ViSA-Flow. If ViSA-Flow exhibits these properties, particularly cross-domain alignment, then the underlying dynamics of a manipulation task, when modeled in the ViSA-Flow space $Z_{\text{ViSA-Flow}}$, should be more consistent across domains than in the raw observation spaces O^S, O^T . Let $T_{task}: Z_{\text{ViSA-Flow}} \times A' \to Z_{\text{ViSA-Flow}}$ represent these shared dynamics (where A' might be an abstract action space). A generative model $g_\phi(z_{t+1}|z_{\leq t},l)$ trained on sequences $\{z_t^S\}$ extracted from the large source dataset D_v can learn a prior distribution capturing T_{task} . This learned prior, encoded in the parameters ϕ , encapsulates structural knowledge about manipulation dynamics. When learning the target policy $\pi_\theta(a_t|z_{\leq t}^T,s_{\leq t},l)$ using the limited target data D_τ , initializing with or regularizing towards the pre-learned prior g_ϕ can significantly accelerate learning and improve data efficiency, as the model only needs to adapt the general dynamics to the specific target embodiment and refine the action mapping, rather than learning the dynamics entirely from the scarce target data.

A.2 Hyper-parameter Details

Table 3 lists the hyperparameters used in Section 3. The window sizes h, k, and n set the length of recent ViSA-Flow representations, action chunk, and forward-prediction horizon, respectively. Loss weights $\lambda_{\rm fwd}$ and $\lambda_{\rm prog}$ balance action learning against auxiliary objectives; we down-weight the forward term during fine-tuning so the optimizer focuses on the action chunk prediction. Table 4 shows the hyper-parameters for training ViSA-Flow in different stages. Training (both pre-training and all fine-tuning) was performed on a single NVIDIA RTX 4090 GPU.

Table 3: Key hyper-parameters used for the design of ViSA-Flow architecture.

Hyper-parameter	Pre-train	Fine-tune (CALVIN)	Fine-tune (Real world)
Predicted action length k		5	10
Past observation length h	10	10	10
Predicted ViSA-Flow length n	3	3	3
ViSA-Flow loss ratio λ_{fwd}	1.0	0.1	0.1
Progress loss ratio λ_{prog}	_	1.0	1.0

Table 4: Hyper-parameters for pre-training and fine-tuning ViSA-Flow model.

Hyper-parameter	Pre-train	Fine-tune (CALVIN)	Fine-tune (Real world)
Batch size	32	16	16
Base learning rate	3.6×10^{-4}	3.6×10^{-4}	3.6×10^{-4}
Minimum LR scale	1×10^{-2}	1×10^{-2}	1×10^{-2}
Weight decay	0.0	0.0	0.0
Optimizer	Adam	Adam	Adam
Adam β_1	0.9	0.9	0.9
Adam β_2	0.999	0.999	0.999
Warm-up epochs	5	5	5
Training epochs	30	20	30 (single-stage), 50 (long-horizon)